Hindawi
International Journal of Photoenergy
Volume 2022, Article ID 4053105, 21 pages
https://doi.org/10.1155/2022/4053105

Research Article

Experimental Study on Gas-Solid Heat Transfer Characteristics for the Vertical Waste Heat Recovery Using the Inverse Problem Method

Sizong Zhang,[1] **Zhi Wen**,[1] **Yi Xing**,[1] **Xunliang Liu**,[1] **Hui Zhang**,[1] **and Yaxuan Xiong**[2]

[1]*School of Energy and Environmental Engineering, University of Science and Technology Beijing, Beijing 100083, China*
[2]*Key Laboratory of HVAC, Beijing University of Civil Engineering and Architecture, Beijing 100044, China*

Correspondence should be addressed to Sizong Zhang; zhangsizong@ustb.edu.cn and Yaxuan Xiong; xiongyaxuan@bucea.edu.cn

Received 14 April 2022; Revised 8 September 2022; Accepted 19 September 2022; Published 10 October 2022

Academic Editor: Alberto Álvarez-Gallegos

To establish an accurate model to optimize the vertical cooling process of the sinter, the inverse problem method is used to calculate the gas-solid heat transfer coefficient based on the gas outlet temperature, which is fitted into the correlation. The research indicates that the increase in the gas velocity is beneficial to the enhancement of the gas-solid heat transfer. With the gas velocity u_g increasing from 0.8 m·s^{-1} to 1.6 m·s^{-1}, the heat transfer coefficient h_v increases by about twice. But this effect will weaken with the increase in the particle size. Besides, the reduction of the particle size is conducive to improving the convective heat transfer intensity between the gas and solid. With the particle size decreasing, this enhancement effect is progressively evident. At u_g of 0.8 m·s^{-1}, the increasing extent of h_v is 1142.25 W·m^{-3}·K^{-1} with the particle size decreasing from 20~25 mm to 15~20 mm, while that is 3152.65 W·m^{-3}·K^{-1} with the particle size decreasing from 15~20 mm to 10~15 mm. In addition, the variation of the measured value of the Nusselt number with the Reynolds number has the same trend as predicted values obtained by other works. However, there is a considerable deviation in the value. Among them, the minimum value of the mean relative error is 26.81%. It is proved that the previous empirical correlations are no longer applicable, while the predicted value of this work is in good agreement with the measured value with the mean deviation of only 7.61%. Therefore, the modified correlation can accurately predict the gas-solid heat transfer characteristics in the sinter bed, which lays a foundation for the numerical design and optimization of the new process.

1. Introduction

In 2020, China has formulated the strategy of the "double Carbon." The targets of the Carbon Peak and Carbon Neutrality will be achieved in 2030 and 2060, respectively. It brings the opportunity for the development of the clean energy industry, including the solar and wind energy. Meanwhile, it has brought great challenges to the traditional industry, such as the iron and steel industry. With the formulation of the "double Carbon" strategy, the energy conservation and emission reduction have become the main theme of the development of the iron and steel industry. Although a number of advanced technologies of the energy-saving and emission reduction have been applied [1–4], the energy consumption and pollutant emission in the iron and steel industry still account for the high proportion in the whole industry, especially in the sintering process [5, 6]. Moreover, the waste heat utilization rate of the sintering process is far lower than the international level. Therefore, the waste heat utilization technology of the sinter has become an important focus for the green development of the iron and steel industry.

However, the waste heat recovery rate of the annular cooling process is less than 30% [7], as shown in Figure 1(a). Therefore, the sinter vertical cooling process [7] has been proposed recently based on the coke dry quenching process [8], as shown in Figure 1(b). The vertical process transforms the heat transfer mode from the cross flow to the countercurrent flow by changing the cooler from the horizontal structure to the vertical structure [9].

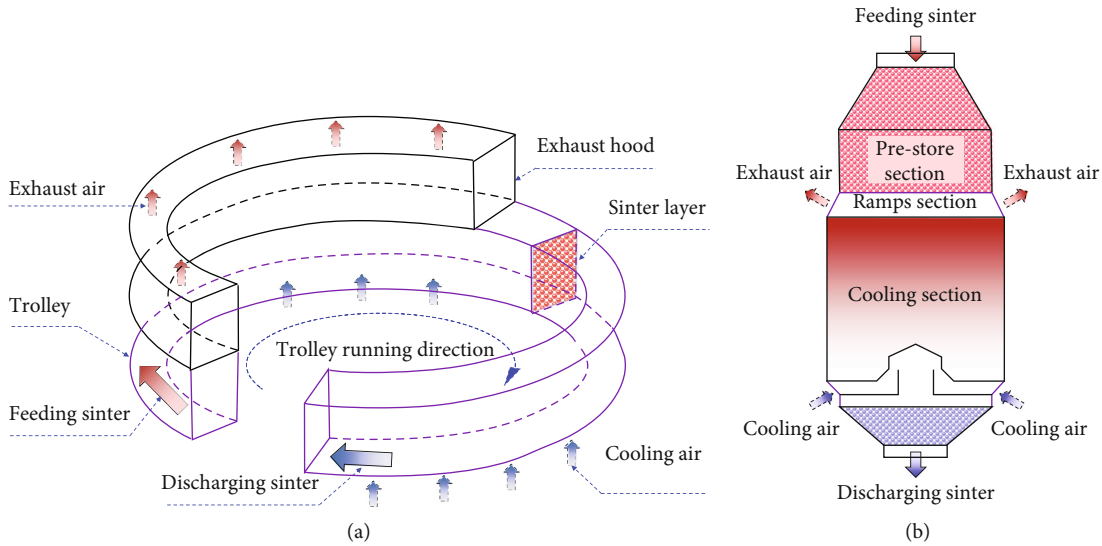

Figure 1: Comparison of two kinds of the sinter waste heat recovery processes: (a) annular cooling process; (b) vertical cooling process.

Moreover, the new process can increase the recovery rate of the waste heat to about 80%, increase the outlet temperature of the exhaust gas from 150~380°C to 500~550°C, and reduce the air leakage rate from 35~50% to nearly zero [7]. Therefore, the application of the new process is one of the important ways to improve the energy-saving and emission reduction of the iron and steel industry.

However, there are few engineering cases of the successful application at present. In addition, the test run indicates that the outlet temperatures of the sinter and exhaust gas are higher and lower than the expected value, respectively [10]. This not only causes the reduction of the sinter treatment capacity but also decreases the recovery rate and quality of the waste heat. It can be attributed to the unreasonable design of the structure and operating parameters, which reduces the heat transfer efficiency in the vertical furnace. The characteristics of the flow resistance and heat transfer are the basis of the design and optimization for the process parameter, which significantly affects the feasibility of the new process [11]. At present, a lot of work has been carried out on the experimental study of resistance characteristics in the sinter bed, and the applicable resistance correlation has been obtained [12–21]. First of all, Liu et al. considered the irregularity of the sinter to modify the resistance correlation [12]. Tian et al. also found that the flow regime in the sinter bed was very easy to be destroyed. Its turbulent degree was higher than the spherical particle, which led to a great increase in the resistance [16]. Besides, Feng et al. corrected the resistance coefficient by using the bed voidage and found that the critical Reynolds number increased as a third-order relationship with the increase of the particle diameter [13]. In addition, it was found that the pressure drop was basically the same along the radial direction except at the wall. Therefore, the wall effect was considered for the correlation correction [14, 15]. What's more, the influence of the wall on the gas flow decreased with the increase of the irregularity of the sinter [17]. In addition, Pan et al. found that the addition of the small-size sinter (0~10 mm) led to the increase of the resistance by 2~3 times [18]. Therefore, Zhang et al. considered the effect of the particle size distribution to correct the resistance correlation [19–21]. It was also found that the resistance in the sinter bed with the narrow particle size distribution is lower than that with the wide particle size distribution.

In addition, many scholars have done a lot of research on gas-solid heat transfer characteristics in the particle bed and obtained the corresponding heat transfer correlations [22–29], as shown in Table 1. First of all, Ranz et al. fitted the heat transfer correlation applicable to the packed bed of the single particle layer [27]. Wakao et al. further considered the influence of the axial fluid heat dispersion to modify the heat transfer correlation of the spherical particles [22]. What's more, Gputa et al. found that the heat transfer factor depended not only on the particle Reynolds number but also on the bed void [23, 24]. To reduce the scattering degree between the experimental data and the fitting value, the bed voidage should be introduced to modify the correlation [24]. However, Singhal et al. thought that previous studies did not consider very dense particle ensembles, i.e., having the bed voidage of less than 0.4 [28]. Previous correlations were more suitable for fluidized beds than packed beds. For large particles, the gas-particle heat transfer in packed beds was typically a much more important limiting factor than in fluidized beds. Therefore, Singhal et al. present a new numerical methodology for deriving heat transfer correlations of very dense particle packed beds [28]. In addition, Will et al. corrected the correlation by considering the thermal radiation and natural convection and expanded the application range of the Reynolds number [29]. It was also found that when the Reynolds number was greater than 2.9×10^5, the heat transfer coefficient suddenly increased. Besides, the studies of Ref. [30–33] indicated that the packing structure of particles had a significant impact on the heat transfer. The comprehensive heat transfer performance of the ordered packing mode is better than that of the disordered packing mode. In the ordered packing mode, the gas

Table 1: Summary of previous correlations in the Nusselt number form for the gas-solid heat transfer in the particle packed bed.

Researcher	Heat transfer correlation	Equation
Wakao et al. [22]	$Nu = 2 + 1.1\mathrm{Re_p}^{0.6}\mathrm{Pr}^{1/3}$	(1)
Thodos et al. [23]	$Nu = (1/\varepsilon)\left(2.876 + 0.3023\mathrm{Re_p}^{0.65}\right)\mathrm{Pr}^{1/3}$	(2)
Gputa et al. [24]	$Nu = (1/\varepsilon)\left(0.0108 + \left(0.929/\mathrm{Re_p}^{0.65} - 0.483\right)\right)\mathrm{Re_p}\mathrm{Pr}^{1/3}$	(3)
Ramos et al. [25]	$Nu = 2 + 0.7\mathrm{Re_p}^{0.5}\mathrm{Pr}^{1/3}$	(4)
Handley and Heggs [26]	$Nu = (1/\varepsilon)0.255\mathrm{Re_p}^{2/3}\mathrm{Pr}^{1/3}$	(5)
Ranz [27]	$Nu = 2 + 0.6\mathrm{Re_p}^{0.5}\mathrm{Pr}^{1/3}$	(6)
Singhal et al. [28]	$Nu = 2.67 + 0.53\mathrm{Re_p}^{0.77}\mathrm{Pr}^{0.53}$	(7)
Will et al. [29]	$Nu = 2 + 0.493\mathrm{Re_p}^{1/2} + 0.0011\ \mathrm{Re_p}$	(8)

channel is more uniform, which makes the gas-solid contact more sufficient. Yang et al. [30, 34] and Wu et al. [31] also analyzed the influence of the particle size distribution. They found that the temperature field and flow field in the bed with non-uniform particles were more uneven than that of uniform particles. It resulted in a significant reduction in the comprehensive heat transfer performance. This may be attributed to that the packing structure of non-uniform particles is more disordered than that of uniform particles.

However, the previous research mainly focuses on spherical or regular particles, while there are few studies on the extremely irregular particles such as the sinter. Also, Yang [35, 36] found that the bed of ellipsoidal particles not only had lower gas resistance than the spherical particle bed but also had higher heat transfer performance. In addition, Tavasoli et al. [37] showed that the heat transfer correlation of spherical particles could be applied to spherocylinder particles only by modifying the particle diameter of spherocylinder. The above research indicates that the influence of the particle shape on the heat transfer cannot be ignored, and the previous correlation of regular particles is no longer applicable. Therefore, it is very necessary to study the gas-solid heat transfer characteristics in the irregular sinter bed.

In recent years, scholars have also carried out some related research on the heat transfer characteristics of the sinter. First of all, Zheng et al. [9] obtained the gas-solid heat transfer coefficient of the sinter by the logarithmic mean temperature difference (LMTD) method with using the moving bed. It can be found that the change trend of the heat transfer coefficient with the Reynolds number was consistent with the predicted value of Wakao's correlation [22]. However, there was a large deviation in the value, which was caused by the difference of the particle shape. Due to the limitation of the discharge device, the particle size range in the study was only 5~20 mm, which was far smaller than the typical particle size in the actual engineering production. Besides, Jang and Chiu [38] proposed the heat transfer correlation by combining experiment and numerical methods. But it was aimed at the cross-flow heat exchange mode of the annular cooling process. This was not suitable for the countercurrent heat exchange mode of the vertical cooling process. In addition, Pan et al. [18], Huang et al. [39], and Feng et al. [40] used the fixed bed to study the heat transfer characteristics of the sinter based on LMTD method, and put forward the heat transfer correlation. When calculating the heat transfer coefficient by LMTD method, the arithmetic mean of the inlet and outlet temperatures was regarded as the average temperature of the whole bed. They considered that the temperature in the bed changed linearly with the height, which was inconsistent with the actual situation of the exponential change. Based on the above shortcomings, this paper studies heat transfer characteristics of the sinter with the typical particle size in the actual production by using the fixed bed. The inverse heat transfer problem method [41–43] is adopted to calculate the heat transfer coefficient, which is fitted as the heat transfer correlation suitable for the sinter.

2. Experimental Method and Data Processing

2.1. Experimental Apparatus and Procedure. To measure the temperature during the cooling process of the sinter, a hot test-bed is constructed, as shown in Figure 2. The test-bed consists of five parts, which are the packed bed, air supply system, heating control system, measurement system, and data acquisition system, respectively. Firstly, the inner diameter and height of the packed bed are 209 mm and 900 mm, respectively. Secondly, the air supply system includes the frequency conversion blower and two ball valves. The flow rate and flow direction of the gas can be controlled by adjusting the blower frequency and valve switch, respectively. Thirdly, the heating control system includes the temperature control cabinet, two temperature-controlled thermocouples, and electric heating wire. The sinter is heated to the design temperature by controlling the heating program. Fourthly, the measurement system is composed of the vortex flowmeter and K-type thermocouples, which are used to measure the flow rate of the gas and the temperature of the gas and solid, respectively. Fifthly, the data acquisition system is the Agilent data acquisition instrument, recording the temperature and flow rate of the gas during the cooling process.

The sinter used in the experiment comes from the production site of an iron and steel company. After screening, the heat transfer characteristics of seven kinds of typical particle sizes [16, 20, 21] are studied, as shown in Table 2. The equivalent particle diameter and bed voidage

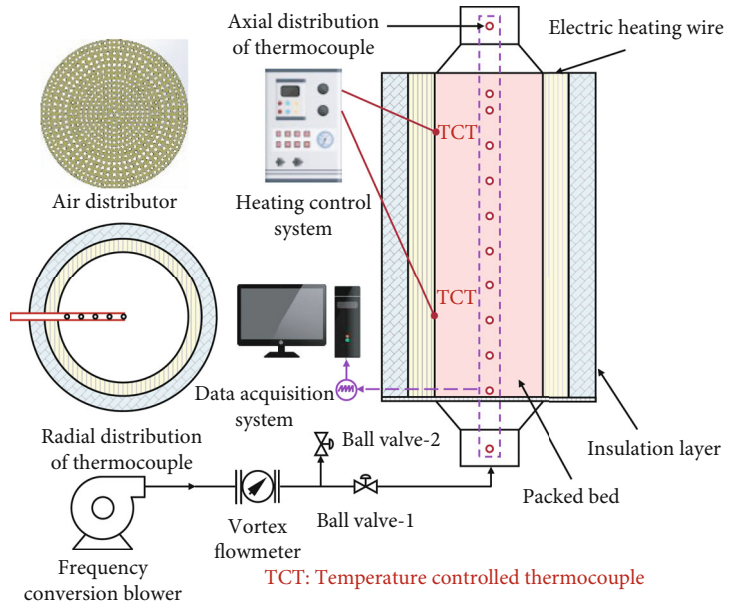

Figure 2: Schematic diagram of the gas-solid heat transfer test-bed for the sinter.

Table 2: Experimental conditions and characteristic parameters for 7 kinds of particle sizes.

Particle size d (mm)	Equivalent particle diameter d_p (mm)	Bed voidage ε	Bed height L (m)	Gas velocity u_g (m·s^{-1})
5~10	5.76	0.5728	0.5673	0.8, 1.0, 1.2, 1.4, 1.6
10~15	11.11	0.5939	0.6162	0.8, 1.0, 1.2, 1.4, 1.6
15~20	14.72	0.6038	0.6434	0.8, 1.0, 1.2, 1.4, 1.6
20~25	19.50	0.6073	0.6576	0.8, 1.0, 1.2, 1.4, 1.6
25~30	23.55	0.6118	0.6748	0.8, 1.0, 1.2, 1.4, 1.6
35~40	30.97	0.6203	0.6945	0.8, 1.0, 1.2, 1.4, 1.6
45~50	38.80	0.6293	0.7149	0.8, 1.0, 1.2, 1.4, 1.6

are characterized by the equal volume method and weighing method, respectively [19, 20]. To provide accurate thermophysical properties for the calculation of the heat transfer coefficient, Figure 3 shows the specific heat and thermal conductivity of the sinter measured by the methods of the scanning calorimetry and laser flash, respectively. Besides, the mass and heating process under different particle sizes are the same to ensure the comparability of the experimental results. First of all, the sinter is heated from the room temperature to 500°C at the heating rate of 10 K·min^{-1}. Secondly, it is kept at 500°C for 3 h. Then, the gas is blown into the bed at the set flow rate to cool the sinter for 1 h. During the cooling process, the gas outlet temperature shall be recorded as the original data for calculating the heat transfer coefficient. Finally, the above process is repeated to measure the gas outlet temperature under different flow rates and particle sizes, so as to analyze the influence of the flow rate and particle size.

2.2. Calculation Method of the Volumetric Heat Transfer Coefficient. The sinter cooling process is essentially the forced convection heat transfer of the gas in the porous medium formed by the accumulation of sinter particles, as shown in Figure 4.

Therefore, this paper adopts the inverse heat transfer problem method in the porous media [41–43] to calculate the heat transfer coefficient. First of all, the forward problem model is established based on the reasonable assumptions:

(1) It is considered that the gas flows only along the axial direction of the bed, ignoring the heat transfer in the circumferential and radial directions. Therefore, the cooling process can be regarded as the one-dimensional unsteady process

(2) The bed formed by the accumulation of sinter particles can be regarded as the homogeneous and isotropic porous medium

(3) The heat transfer between the sinter and air is carried out by the convection, which is in the local non-thermal equilibrium

According to the above assumptions, the following mathematical model can be established [41–43].

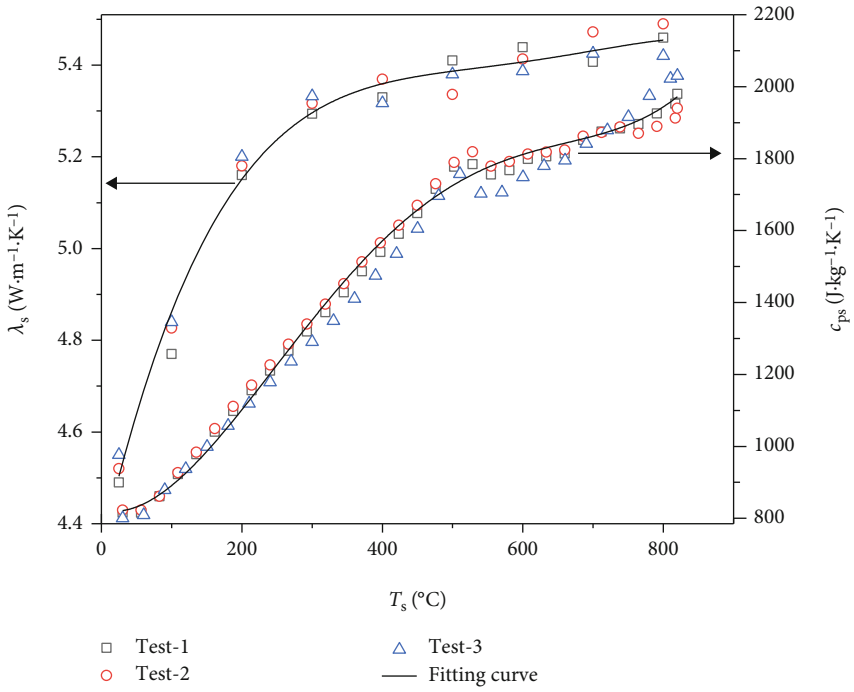

Figure 3: Measured data of the thermal conductivity λ_s and specific heat c_{ps} of the sinter at different temperatures.

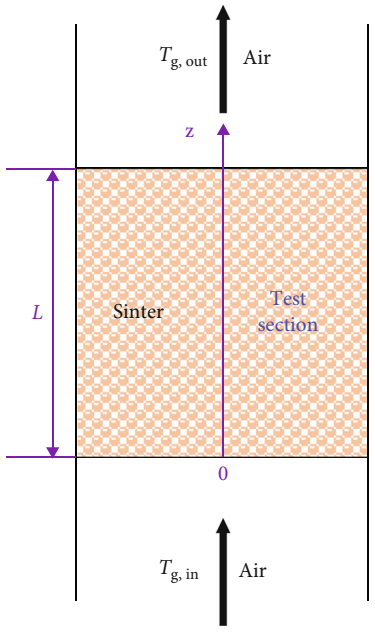

Figure 4: Schematic diagram of the physical model for the sinter cooling process.

(1) Energy equation of the gas:

$$\frac{\partial\left(\varepsilon\rho_g c_{pg} T_g\right)}{\partial t} + \frac{\partial\left(\varepsilon\rho_g v_g c_{pg} T_g\right)}{\partial z} = \varepsilon\frac{\partial}{\partial z}\left(\lambda_g \frac{\partial T_g}{\partial z}\right) + h_v\left(T_s - T_g\right), \quad (1)$$

where ρ_g is the density of the gas, kg·m^{-3}; c_{pg} is the specific heat of the gas, J·kg^{-1}·°C^{-1}; λ_g is the thermal conductivity of the gas, W·m^{-1}·°C^{-1}; T_g is the temperature of the gas, °C; T_s is the temperature of the sinter, °C; h_v is the volumetric heat transfer coefficient, W·m^{-3}· °C^{-1}.

(2) Energy equation of the sinter:

$$\frac{\partial\left((1-\varepsilon)\rho_s c_{ps} T_s\right)}{\partial t} = (1-\varepsilon)\frac{\partial}{\partial z}\left(\lambda_s \frac{\partial T_s}{\partial z}\right) + h_v\left(T_g - T_s\right), \quad (2)$$

where ρ_s is the density of the sinter, kg·m^{-3}; c_{ps} is the specific heat of the sinter, J·kg^{-1}·°C^{-1}; λ_s is the thermal conductivity of the sinter, W·m^{-1}·°C^{-1}.

At the beginning of the cooling process, the temperature of the gas and solid is the same, which is the temperature measured by the thermocouple at the end of the insulation stage. The boundary conditions of energy equations for the gas and solid are as follows:

$$\begin{aligned} T_g(t, z=0) &= T_{g,in}, \\ -(1-\varepsilon)\lambda_s \frac{\partial T_s(t, z=0)}{\partial z} &= h_v\left(T_{g,in} - T_s(t, z=0)\right), \\ \lambda_g \frac{\partial T_g(t, z=L)}{\partial z} &= 0, \\ \lambda_s \frac{\partial T_s(t, z=L)}{\partial z} &= 0, \end{aligned} \quad (3)$$

where $T_{g,in}$ is the inlet temperature of the gas, which is the same as the ambient temperature, °C.

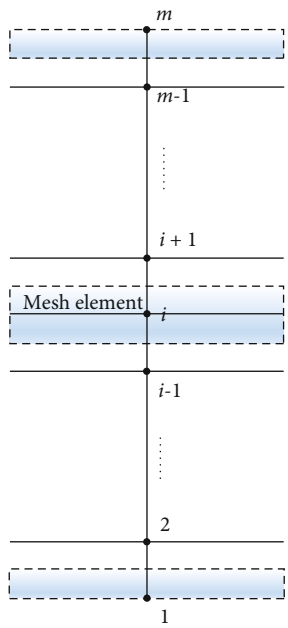

Figure 5: Schematic diagram of the mesh discretization of the physical model.

Next, the method of the numerical solution is introduced. First of all, the physical model is discretized by the outside node method to determine the mesh element, node position, and control volume, as shown in Figure 5.

Besides, the energy equation is discretized by the control volume integration method to obtain the discrete equation. The algebraic equation of each element after discretization is shown in Eqs. (4) and (5).

(1) Discretization equation of the gas:

$$\begin{aligned}&\left[\varepsilon_i\left(\rho_g c_{pg}\right)_i^{j-1}\Delta z+\left(\rho_g v_g\right)_0 c_{pg,i}^{j-1}\Delta t+\varepsilon_i\lambda_{g,i+1}^{j-1}\frac{\Delta t}{\Delta z}+\varepsilon_i\lambda_{g,i-1}^{j-1}\frac{\Delta t}{\Delta z}+h_v\Delta t\Delta z\right]\\&\cdot T_{g,i}^{j}-\left[\varepsilon_i\lambda_{g,i-1}^{j-1}\frac{\Delta t}{\Delta z}+\left(\rho_g v_g\right)_0 c_{pg,i-1}^{j-1}\Delta t\right]T_{g,i-1}^{j}-\varepsilon_i\lambda_{g,i+1}^{j-1}\frac{\Delta t}{\Delta z}T_{g,i+1}^{j}\\&=\varepsilon_i\left(\rho_g c_{pg}\right)_i^{j-1}\Delta z T_{g,i}^{j-1}+h_v\Delta t\Delta z T_{s,i}^{j-1}.\end{aligned}\tag{4}$$

(2) Discretization equation of the solid:

$$\begin{aligned}&\left[(1-\varepsilon_i)\left(\rho_s c_{ps}\right)_i^{j-1}\Delta z+(1-\varepsilon_i)\lambda_{s,i+1}^{j-1}\frac{\Delta t}{\Delta z}+(1-\varepsilon_i)\lambda_{s,i-1}^{j-1}\frac{\Delta t}{\Delta z}+h_v\Delta t\Delta z\right]\\&\cdot T_{s,i}^{j}-(1-\varepsilon_i)\lambda_{s,i-1}^{j-1}\frac{\Delta t}{\Delta z}T_{s,i-1}^{j}-(1-\varepsilon_i)\lambda_{s,i+1}^{j-1}\frac{\Delta t}{\Delta z}T_{s,i+1}^{j}\\&=(1-\varepsilon_i)\left(\rho_s c_{ps}\right)_i^{j-1}\Delta z T_{s,i}^{j-1}+h_v\Delta t\Delta z T_{g,i}^{j-1},\end{aligned}\tag{5}$$

where j and $j-1$ represent this moment and the last moment; $i-1$, i, and $i+1$ represent the last node, this node, and the next node, respectively; Δz and Δt represent the time step and space step, m and s, respectively.

By discretizing the controlling equation of each element, a series of algebraic equations can be obtained to form an algebraic equation system similar to Eq. (6).

$$\begin{cases}b_1x_1+c_1x_2=d_1\\a_2x_1+b_2x_2+c_2x_3=d_2\\\cdots\\a_ix_{i-1}+b_ix_i+c_ix_{i+1}=d_i\\\cdots\\a_{m-1}x_{m-2}+b_{m-1}x_{m-1}+c_{m-1}x_m=d_{m-1}\\a_mx_{m-1}+b_mx_m=d_m\end{cases}.\tag{6}$$

The algebraic equation system is solved by the tridiagonal matrix algorithm (TDMA) based on the Gauss elimination method. Finally, the computer language C# is used to write the calculation program to realize the above algorithm, thereby solving the sinter cooling process.

To obtain the solution independent of the space and time, the temperature field in the bed under different time and space steps is calculated by the numerical model. The change of the gas outlet temperature $T_{g,out}$ with the time is shown in Figure 6. It is found that the change of $T_{g,out}$ is no longer significant when Δz and Δt are less than 0.35 mm and 3 s, respectively. However, the further reduction of the time step and space step would greatly increase the amount of the calculation, while the improvement of the calculation accuracy is limited. Therefore, Δz and Δt are set to 0.35 mm and 3 s in this paper, respectively.

To verify the accuracy of the numerical model, the experimental data in Ref. [39] are compared with the calculated value of this model, as shown in Figure 7. First of all, Figure 7(a) shows that the variation trend of the measured value and calculated value with the time is basically consistent. Besides, Figure 7(b) indicates that the relative error between the measured value and predicted value is less than 5%. Therefore, the numerical model established can well predict the cooling process of the sinter.

Figure 8 shows the whole process of calculating the heat transfer coefficient by using the inverse problem method. Firstly, the value of the convective heat transfer coefficient h_v is assumed. Combined with conditions of the geometric parameters, physical properties, gas inlet temperature, and initial temperatures of the gas and solid, the calculated value of the gas outlet temperature $(T_{g,out})_{cal}$ is solved by the numerical model. Then, the absolute deviation δ is obtained by comparing the calculated value of the gas outlet temperature $(T_{g,out})_{cal}$ with the measured value $(T_{g,out})_{exp}$. If δ is less than 1×10^{-3}, the assumed value is the measured value of the heat transfer coefficient at this moment. Otherwise, the heat transfer coefficient h_v is modified based on the deviation δ between $(T_{g,out})_{cal}$ and $(T_{g,out})_{exp}$ [42]. Using the

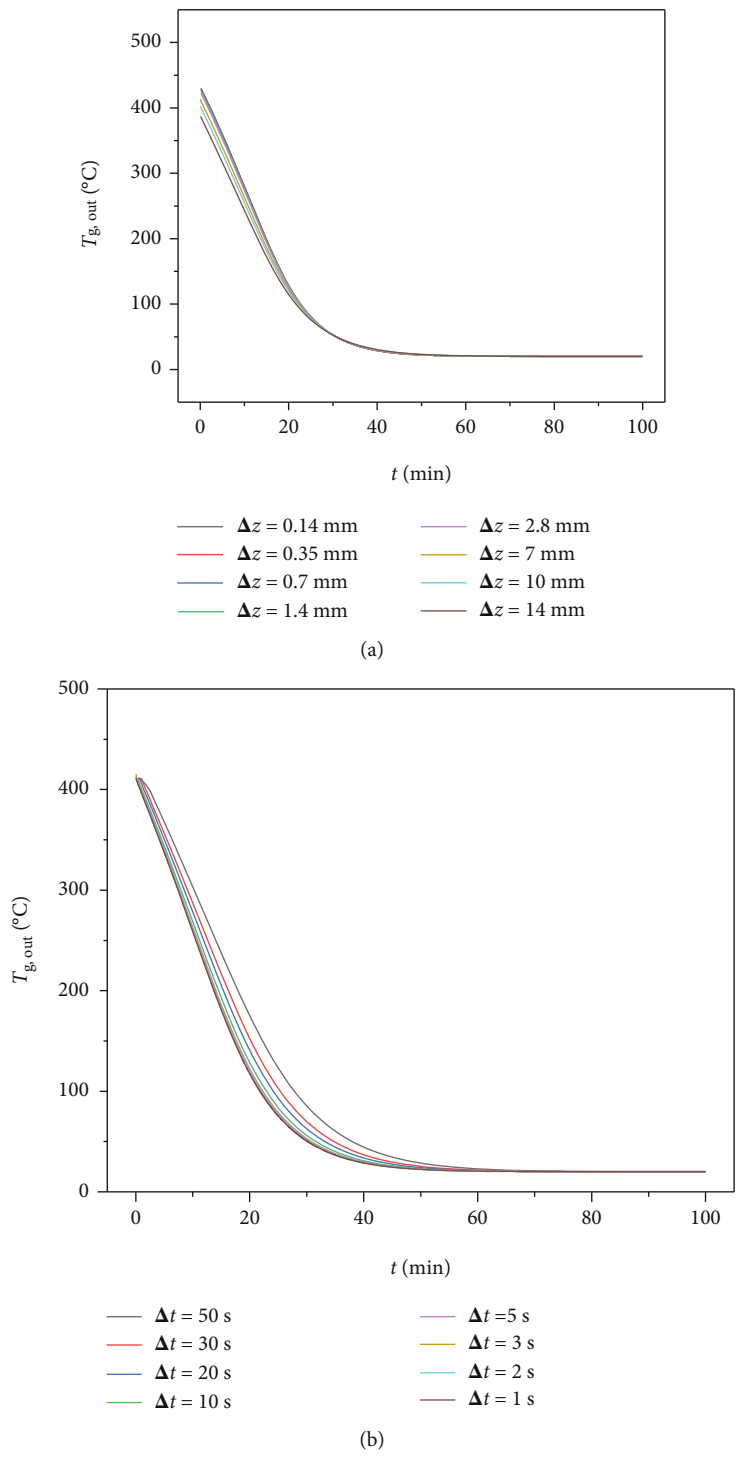

FIGURE 6: The change of the gas outlet temperature $T_{g,out}$ with the time t: (a) different space steps Δz; (b) different time steps Δt.

modified heat transfer coefficient, the energy equation is resolved until δ is less than 1×10^{-3}.

2.3. Analysis of the Uncertainty. Since this paper uses the inverse problem method to calculate the heat transfer coefficient, it is difficult to use the error transfer theory to directly analyze the uncertainty [44]. For the inverse problem method, the uncertainty analysis generally adopts the method of setting the manual error [44]. The error of this experiment mainly comes from the measurement of the temperature, flow rate of the gas, and height of the sinter bed. The measurement accuracy of the thermocouple and flowmeter is class I, and the measurement errors of the temperature and flow rate are 0.4% and 1.0%, respectively.

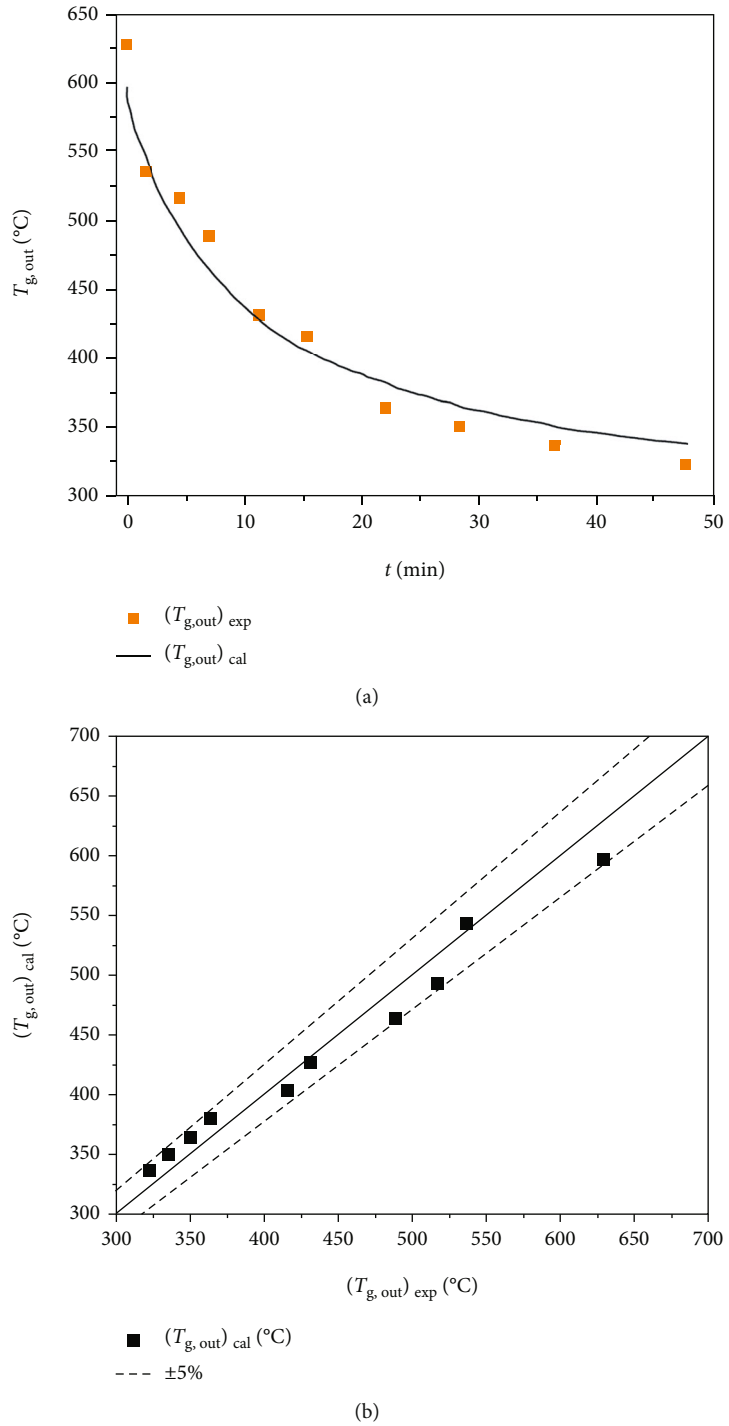

FIGURE 7: Verification of the numerical model: (a) change of the calculated value and measured value of the gas outlet temperature $T_{g,out}$ with time t; (b) comparison between the calculated value $(T_{g,out})_{cal}$ and measured value $(T_{g,out})_{exp}$ of the gas outlet temperature.

The accuracy of the straight rule used to measure the bed height is 1 mm. Since the minimum height of the bed layer of seven kinds of sinters is greater than 500 mm, the maximum error is less than 0.2%. Then, the uncertainty caused by these three parameters on the heat transfer coefficient h_v is analyzed by the method of setting manual error.

First of all, the heat transfer coefficient h_v of three different particle sizes under the gas velocity of 0.8 $m \cdot s^{-1}$ is set, as shown in Figure 9. Based on the heat transfer coefficient, the outlet temperature of the gas is calculated by the numerical model, as shown in Figure 10. Besides, the standard deviation corresponding to the relative error is used to generate the random number of the normal distribution as the

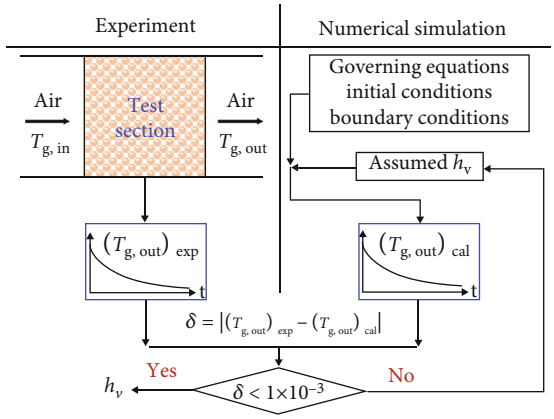

FIGURE 8: The whole process of calculating the heat transfer coefficient by the inverse problem method.

manual error [44]. Then, the error is added to the exact value as the input parameter of the inverse problem to recalculate the heat transfer coefficient. Finally, the influence of the measurement error is estimated by comparing the recalculated heat transfer coefficient with the set value.

The following is a brief description of the temperature measurement error as an example. The gas outlet temperature with the error can be obtained by Eq. (7):

$$\left(T_{g,out}\right)_{err} = \left(T_{g,out}\right)_{exact} + \xi_{T_{g,out}}, \tag{7}$$

where $(T_{g,out})_{exact}$ is the outlet temperature of the gas without the error, ˚C; $(T_{g,out})_{err}$ is the outlet temperature of the gas with the error, ˚C; ξ_{T_g} is the normally distributed random number. The standard deviation σ of the normal distribution function is 0.08, corresponding to the temperature measurement error of 0.4% [44]. Figure 11(a) compares the heat transfer coefficient based on $(T_{g,out})_{exact}$ and $(T_{g,out})_{err}$. It is found that calculation errors of the heat transfer coefficient with the particle size of 5~10 mm, 25~30 mm, and 45~50 mm are 11.75%, 5.13%, and 3.67%, respectively. In addition, the measurement errors of the gas flow rate and bed height are estimated by the same method, as shown in Figures 11(b) and 11(c), respectively. The errors caused by the flow rate on the heat transfer coefficient for the sinters of 5~10 mm, 25~30 mm, and 45~50 mm are 6.11%, 3.96%, and 2.32%, respectively. The errors caused by the bed height for the sinters of 5~10 mm, 25~30 mm, and 45~50 mm are 0.89%, 0.38%, and 0.31%, respectively. The comparison indicates that the temperature measurement has the greatest impact on the heat transfer coefficient, followed by the flow rate of the gas. The influence of the bed height can be almost ignored.

3. Experimental Results and Discussions

3.1. Effect of the Gas Velocity on Gas-Solid Heat Transfer Characteristics. Figure 12 illustrates the change of the gas outlet temperature $T_{g,out}$ and its change rate $dT_{g,out}$ with the cooling time t in the sinter bed of the 5~10 mm under different gas velocities u_g. Since the gas outlet temperature is repeatedly measured three times under each condition, the curve in Figure 12(a) is the average value of the three results. Since the number of experiments is small, the error bar should be calculated by using the t-distribution. The significance level selected in this paper is 0.05, that is, the confidence probability is 95%. Firstly, the t-distribution table shows that $t_{0.05/2}(2)$ is 4.3027. Besides, the standard error $S_{\bar{x}}$ is calculated as follows:

$$S_{\bar{x}} = \sqrt{\frac{\sum_{i=1}^{3}(x_i - \bar{x})^2}{3\times(3-1)}}, \tag{8}$$

where x_i represents the gas outlet temperature measured by each time; $\bar{x}$ represents the mean value of the three results. Therefore, the error bar is $t_{0.05/2}S_{\bar{x}}$, as shown in Figure 12(a).

Firstly, the curve of $T_{g,out}$ moves to the left side of the time axis with the increase of u_g. This indicates that the time required for the cooling process decreases with the increase in u_g. The completion time for the cooling process decreases from about 39 min to 22 min with u_g increasing from 0.8 m·s^{-1} to 1.6 m·s^{-1}, which is shortened by 43.59%. Besides, both the steep degree of the $dT_{g,out}$ curve and the peak value of $dT_{g,out}$ increase with the increase of u_g. The peak value of $dT_{g,out}$ increases from 29.16˚C·min^{-1} to 55.28˚C ·min^{-1} with u_g increasing from 0.8 m·s^{-1} to 1.6 m·s^{-1}, which increases by about 1 time. The above result shows that the increase of u_g is conducive to improve the heat transfer between the gas and solid.

For the cooling process of the sinter, the heat transfer mode between the gas and solid is mainly the convective heat transfer. The viscous force caused by the viscosity occupies an absolute advantage at the wall. This results in the existence of the laminar flow boundary layer on the particle surface, also known as the heat transfer boundary layer. The heat transfer in this area mainly depends on the heat conduction. Due to the small thermal conductivity of the gas, the temperature difference in the laminar flow area is large. Therefore, the heat transfer resistance mainly concentrated in the boundary layer. But the heat transfer in the turbulent region outside the boundary layer mainly depends on the mixing effect caused by the velocity fluctuation. As a result of the violent mixing of fluid particles, there is basically no temperature difference in the turbulent area, which can be considered no heat transfer resistance. Therefore, the thermal resistance of the convective heat transfer mainly depends on the boundary layer. The thicker the boundary layer, the greater the thermal resistance and the weaker the convective heat transfer. The increase of the gas velocity increases the degree of the gas turbulence, which thins the boundary layer and reduces the heat transfer resistance [11]. Consequently, the intensity of the gas-solid convective heat transfer is improved.

Figure 13 shows the change of the mean value $(dT_{g,out})_{mean}$ and peak value $(dT_{g,out})_{peak}$ of the change rate

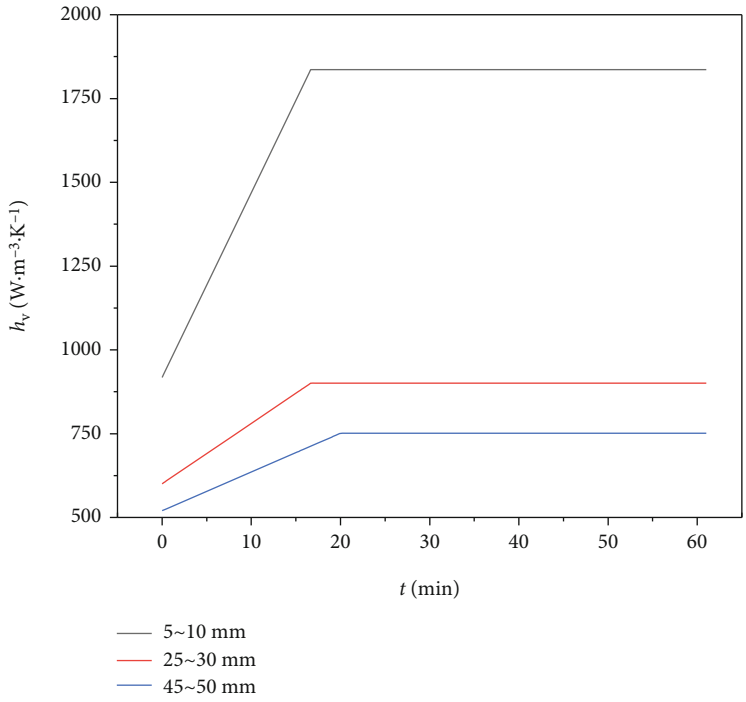

FIGURE 9: Volumetric heat transfer coefficients h_v set for three different kinds of sinters.

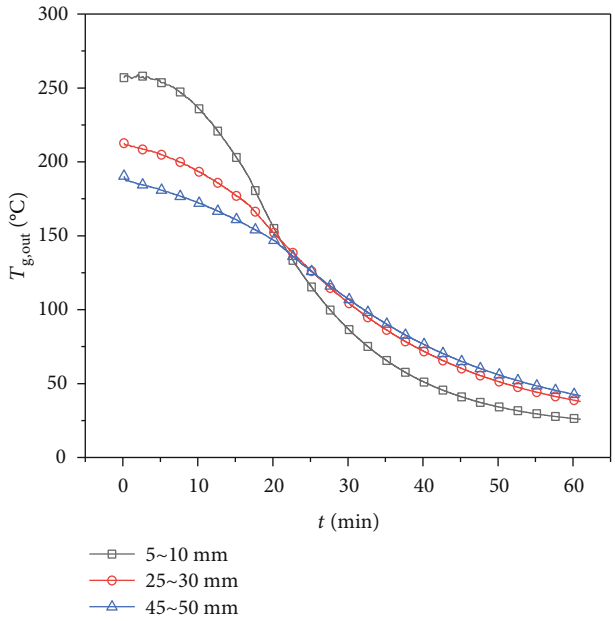

FIGURE 10: Gas outlet temperatures $T_{g,out}$ of three kinds of sinters based on the set heat transfer coefficient.

of the gas outlet temperature with the gas velocity u_g under different kinds of sinters. It is found that the steep degree of the fitting curve reduces with the increase in the particle size. When the particle size increases from 5~10 mm to 45~50 mm, the slopes of the $(dT_{g,out})_{mean}$ curve and $(dT_{g,out})_{peak}$ curve decrease by 55.61% and 70.36%, respectively. This indicates that the increase in the particle size will weaken the effect of the gas velocity on the gas-solid heat transfer. This is attributed to the increase of the heat conduction resistance within the particle [45].

Figure 14 illustrates the variation of the volumetric heat transfer coefficient h_v with the cooling time t in the sinter bed of the 5~10 mm at different gas velocities u_g. Firstly, it is observed that h_v increases with the increase of u_g. At the cooling time of 40 min, h_v increases from 16288 W·m^{-3}·K^{-1}

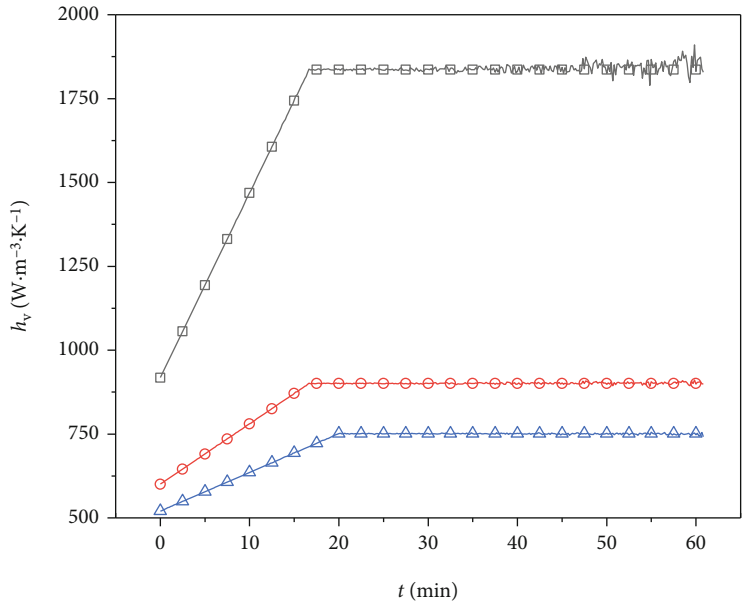

(a)

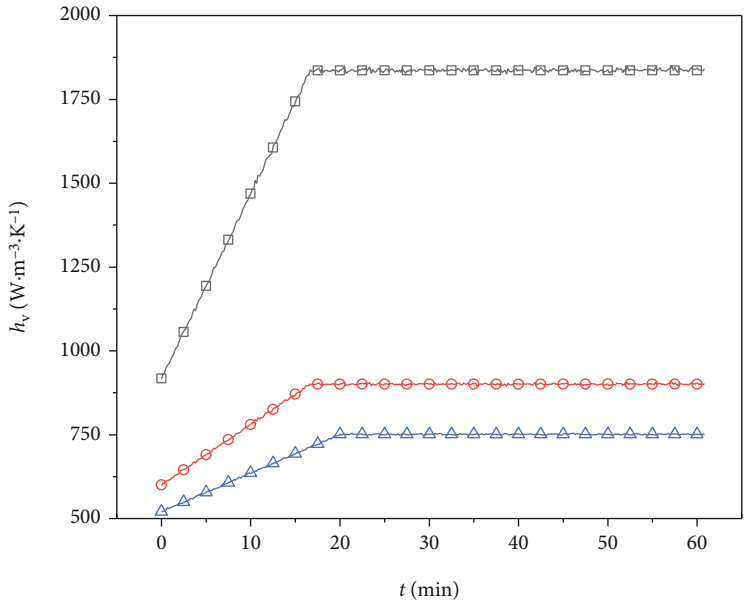

(b)

Figure 11: Continued.

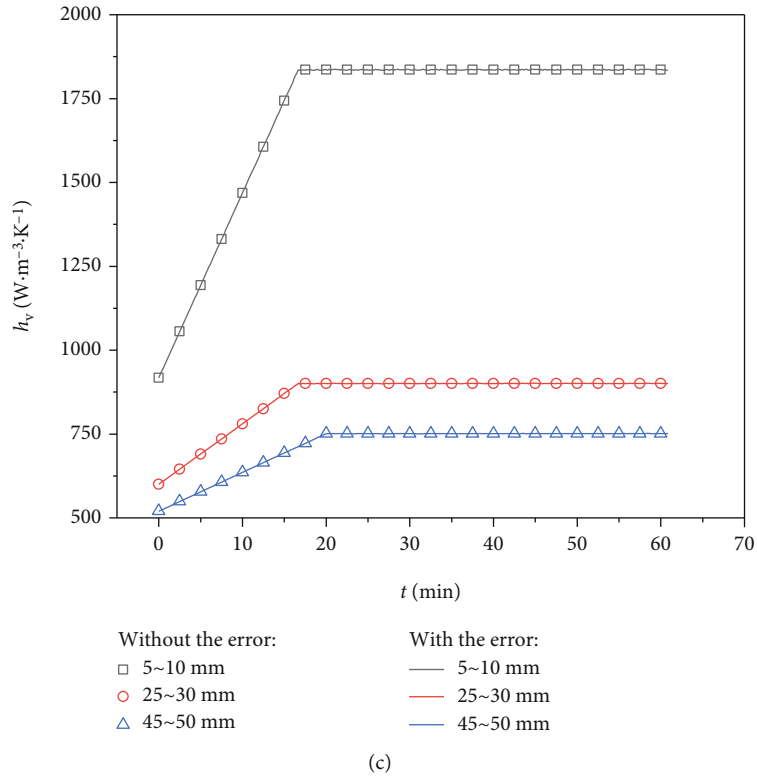

(c)

FIGURE 11: Influence of the measurement error on the heat transfer coefficient h_v: (a) error of the temperature; (b) error of the gas flow rate; (c) error of the bed height.

to 49599 W·m^{-3}·K^{-1} with u_g increasing from 0.8 m·s^{-1} to 1.6 m·s^{-1}, which increases by about twice. Since the turbulent degree of the gas increases with the increase in u_g, the thickness of the boundary layer decreases. This would decrease the thermal resistance. Besides, h_v is smaller in the initial stage of the cooling process but increases gradually with the cooling continuing. Since the gas temperature in the bed is high at the initial stage, the viscosity coefficient is large, which is about 1.8 times that of the room temperature. Therefore, the viscous resistance of the gas on the particle surface increases, which increases the thickness of the boundary layer and heat transfer resistance. As the cooling process continues, the gas temperature decreases. At this time, the viscosity coefficient of the gas decreases, thereby reducing the thickness of the boundary layer. Therefore, the heat transfer resistance decreases, improving the convective heat transfer coefficient. In addition, the greater the gas velocity u_g, the faster the heat transfer coefficient h_v increases in the initial stage. The time of the initial stage at u_g of 0.8 m·s^{-1} and 1.6 m·s^{-1} is about 25 min and 8 min, respectively, which is shortened by 68%. As shown in Figure 12, the decreasing rate of the gas temperature with the cooling time increases with the increase in u_g. This would increase the decreasing range of the viscosity coefficient. Therefore, the faster the gas temperature in the bed decreases with the increase in u_g, the greater the decrease of the viscosity coefficient. Therefore, the decreasing extent of the thickness of the boundary layer increases with the increase in u_g, which makes the increase of the heat transfer coefficient faster in the initial stage.

3.2. Effect of the Equivalent Particle Diameter on Gas-Solid Heat Transfer Characteristics. According to the experimental data under the gas velocity u_g of 0.8 m·s^{-1}, the change curves of the gas outlet temperature $T_{g,out}$ and its change rate $dT_{g,out}$ for sinters with different particle sizes are plotted in Figure 15. Firstly, the smaller the particle size, the higher the gas outlet temperature in the initial stage. At the cooling time of 1 min, $T_{g,out}$ with the particle size of 45~50 mm and 5~10 mm are 305.91°C and 453.54°C with an increase of 147.63°C, respectively. Besides, the steepness of the $dT_{g,out}$ curve increases with the reduction of the particle size, indicating that the time required for cooling is shortened. The cooling time with the particle size of 15~20 mm and 5~10 mm is about 51.5 min and 39.0 min with the reduction of 12.5 min, respectively. In addition, the peak value $(dT_{g,out})_{peak}$ of the $dT_{g,out}$ increases with the particle size decreasing. $(dT_{g,out})_{peak}$ increases from 8.27°C min^{-1} to 29.25°C min^{-1} with the particle size decreasing from 45~50 mm to 5~10 mm, which increases by about 2.5 times. The above results show that the reduction of the particle size is beneficial to improve the intensity of the gas-solid convective heat transfer. This is attributed to the following two main reasons [9, 40, 45]. Firstly, the bed voidage reduces with the decrease in the particle size. It makes the real

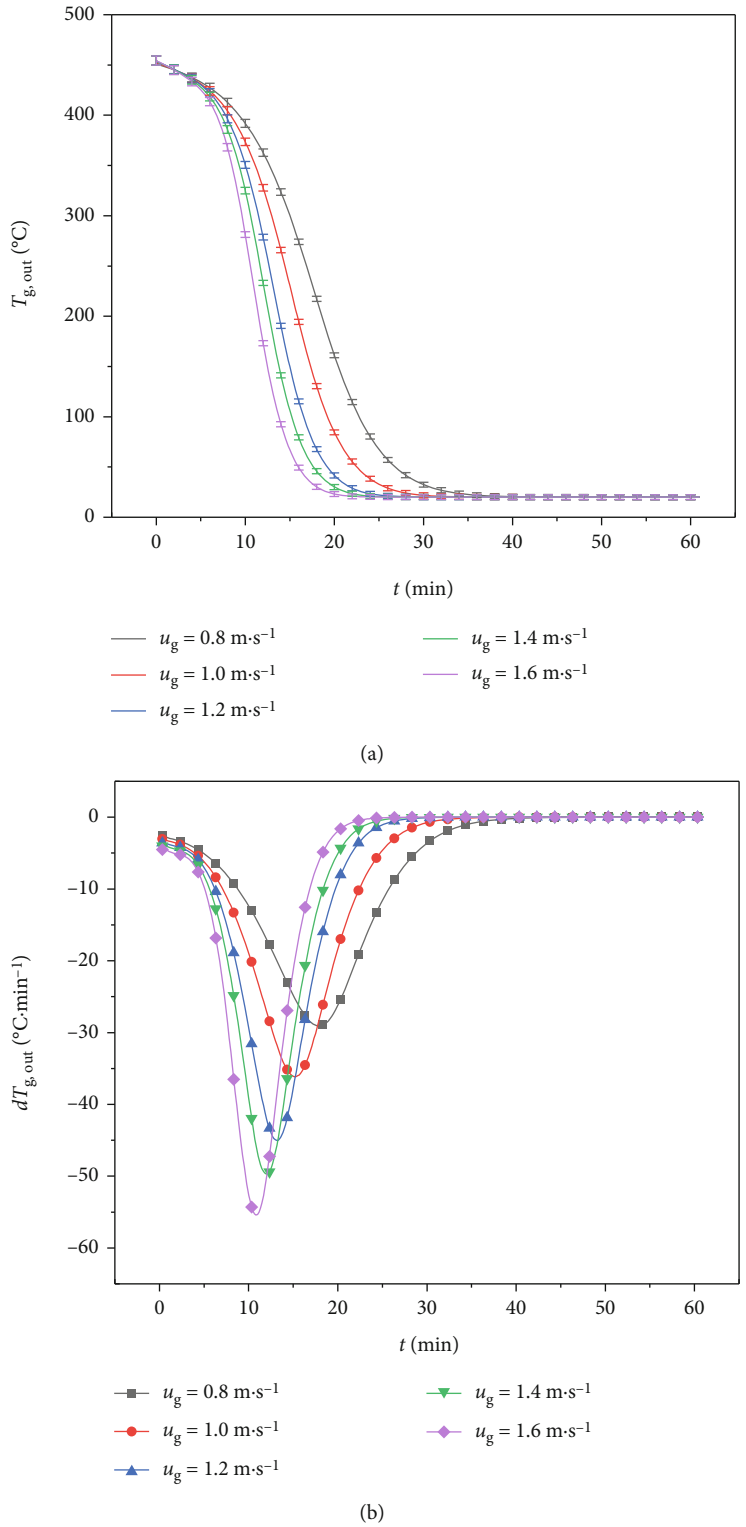

FIGURE 12: Variations of the gas outlet temperature $T_{g,out}$ and its change rate $dT_{g,out}$ with the cooling time t in the sinter bed of the 5~10 mm under different gas velocities u_g.

velocity of the gas in the bed increase under the same flow rate of the gas. Therefore, the boundary layer of the heat transfer will become thin with the increase in the gas turbulence. This makes the thermal resistance decrease. Secondly, the specific surface area of particles increases with the particle size decreasing. It makes the gas-solid contact more sufficient, resulting in an increase in the total heat exchange area.

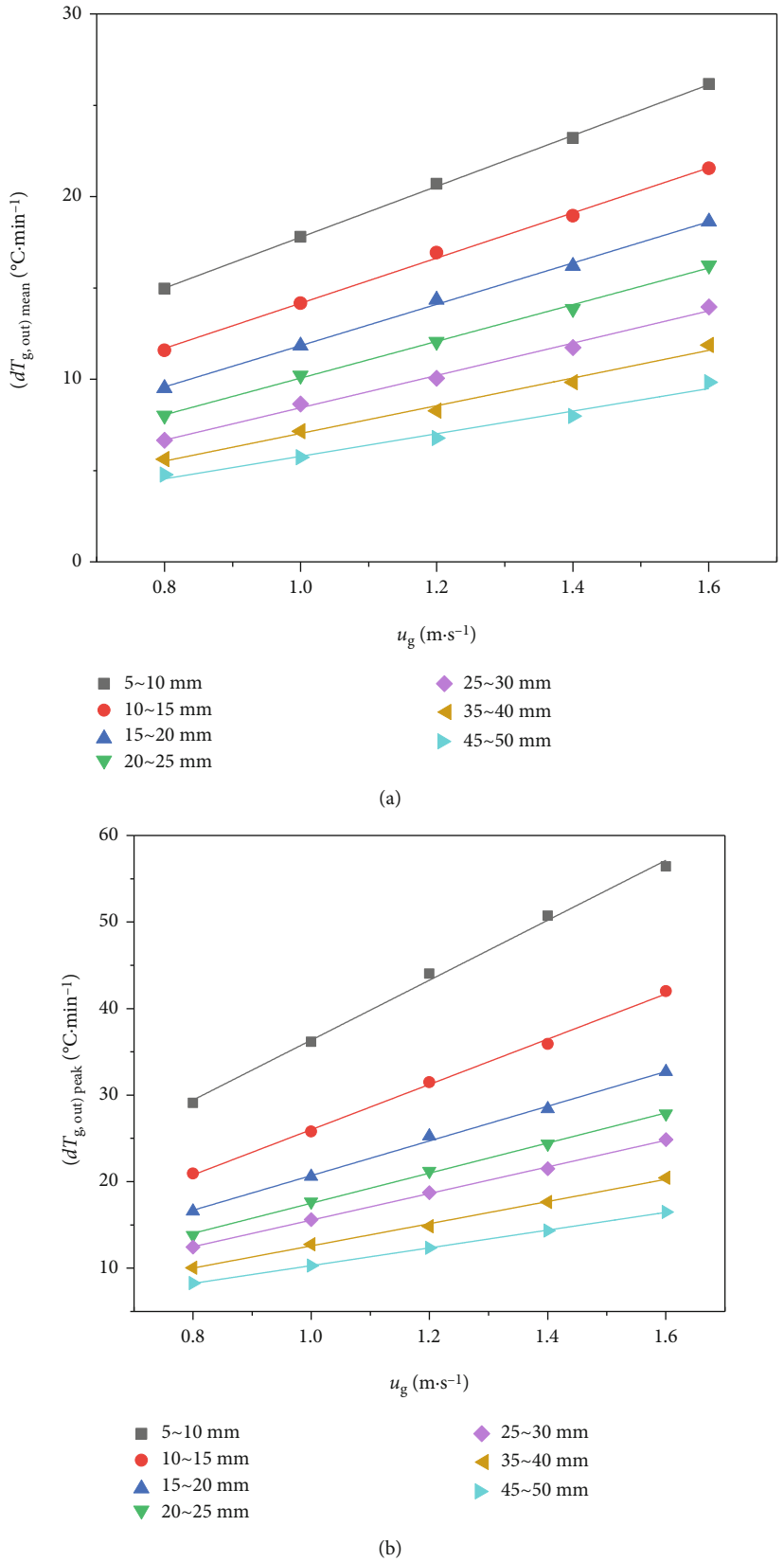

FIGURE 13: Change of the mean value $(dT_{g,out})_{mean}$ and peak value $(dT_{g,out})_{peak}$ of the change rate of the gas outlet temperature with the gas velocity u_g under different kinds of sinters.

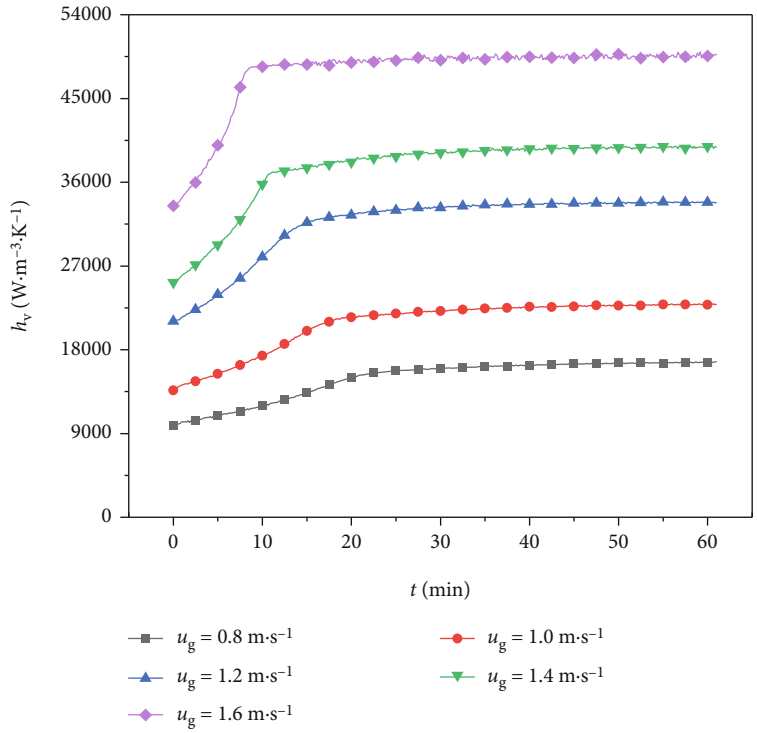

Figure 14: Variation of the heat transfer coefficient h_v of different sinters with the cooling time t at different gas velocities u_g.

Figure 16 illustrates the mean value $(dT_{g,out})_{mean}$ and peak value $(dT_{g,out})_{peak}$ of the change rate of the gas outlet temperature with the equivalent particle diameter d_p under different gas velocities u_g. It can be seen that $(dT_{g,out})_{mean}$ and $(dT_{g,out})_{peak}$ not only increase with the reduction of d_p but also show the growth trend in the increasing extent. In addition, Figure 17 shows that the heat transfer coefficient h_v increases with the reduction of d_p, and the increasing extent also increases. When the sinter is cooled to 40 min, the increasing extent is 1142.25 W·m^{-3}·K^{-1} with the particle size decreasing from 20~25 mm to 15~20 mm, while that is 3152.65 W·m^{-3}·K^{-1} with the particle size decreasing from 15~20 mm to 10~15 mm. The above results indicate that the reduction of d_p is beneficial to improve the gas-solid convective heat transfer, which is more and more significant. First, Figure 18 shows that the specific surface area increases with the particle size decreasing, which makes the gas-solid contact more sufficient. Besides, the reduction in the bed voidage ε with the particle size decreasing makes the turbulent degree of the gas increase. This reduces the heat transfer resistance. Finally, the variation range of the specific surface area and bed voidage also increases with the reduction in the particle size.

4. Modification of the Gas-Solid Heat Transfer Correlation

For the cooling process of the sinter, the main factors affecting the gas-solid heat transfer characteristics include the bed voidage ε, equivalent particle diameter d_p, gas velocity u_g, specific heat of the gas c_{pg}, viscous coefficient of the gas μ_g, thermal conductivity of the gas λ_g, density of the gas ρ_g, and volumetric coefficient of the gas-solid heat transfer h_v. To fit the heat transfer correlation, the following expressions are usually used for the dimensionless treatment of the above factors.

$$Nu = \frac{h_a d_p}{\lambda_g}, \tag{9}$$

where Nu is the Nusselt number representing the intensity of the convective heat transfer; $h_a = h_v/S_{pv}$ is the area heat transfer coefficient of the gas-solid convection, W·m^{-2}·K^{-1}; $S_{pv} = 6(1-\varepsilon)/d_p$ is the specific surface area of particles, m^2·m^{-3}.

$$\mathrm{Pr} = \frac{\mu_g c_{pg}}{\lambda_g}, \tag{10}$$

where Pr is the Prandtl number, which is the ratio of the dynamic viscosity coefficient to the thermal diffusivity.

$$\mathrm{Re}_p = \frac{\rho_g u_g d_p}{\mu_g}, \tag{11}$$

where Re_p is the particle Reynolds number, representing the gas flow state in the particle bed.

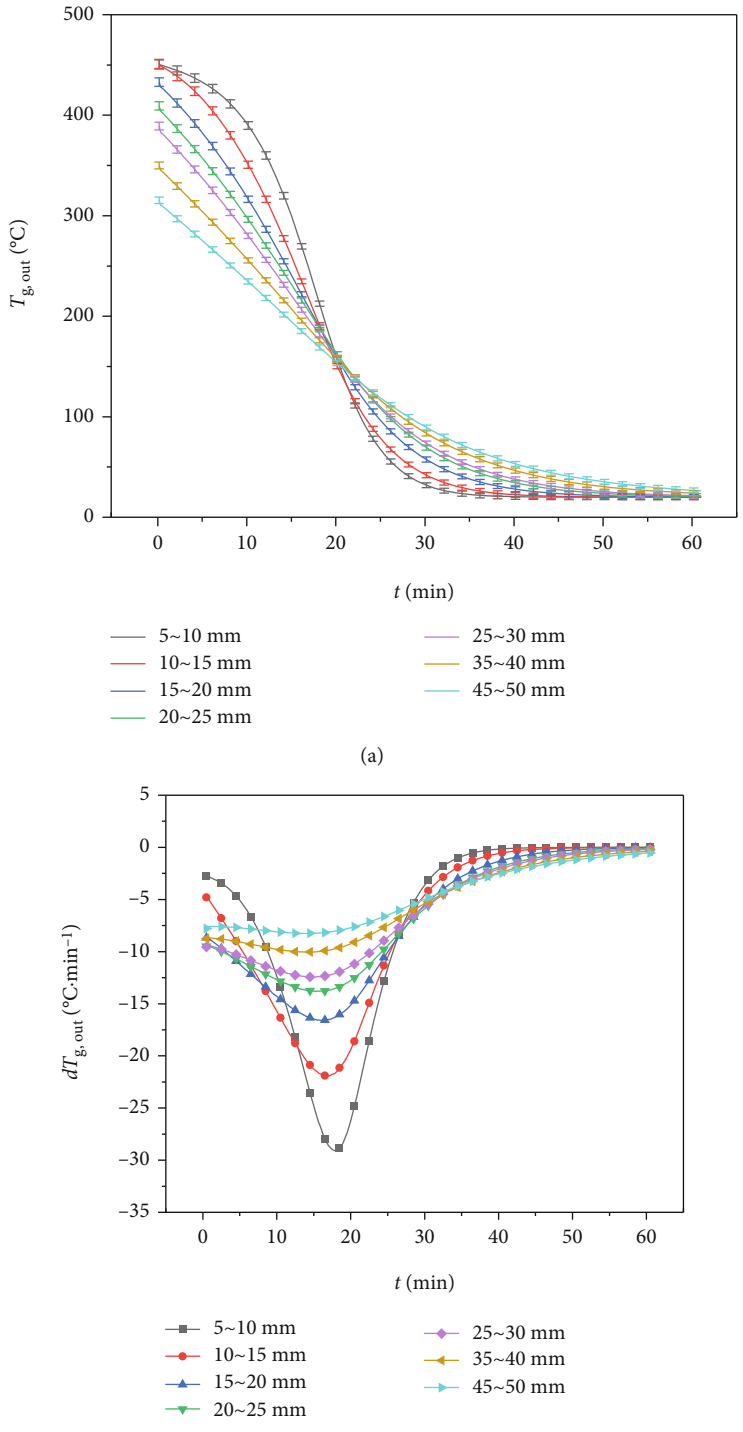

FIGURE 15: Variation of the gas outlet temperature $T_{g,out}$ and its change rate $dT_{g,out}$ with the cooling time t for the different kinds of sinters at the gas velocity of 0.8 m·s^{-1}.

Based on the form of previous correlations [23, 24, 26], the dimensionless gas-solid heat transfer correlation of the sinter is fitted according to the experimental data as follows:

$$Nu = \frac{1}{\varepsilon^{0.356}}\left(1.779 + 0.0256\mathrm{Re_p}^{0.851}\right)\mathrm{Pr}^{1/3}. \quad (12)$$

The fitting correlation coefficient R^2 of the above formula is 0.99015. Figure 19 compares the measured value of the Nusselt number Nu with the predicted value calculated by this work and other works. Furthermore, the comparison is made by means of the mean relative deviation (MRD), as given by

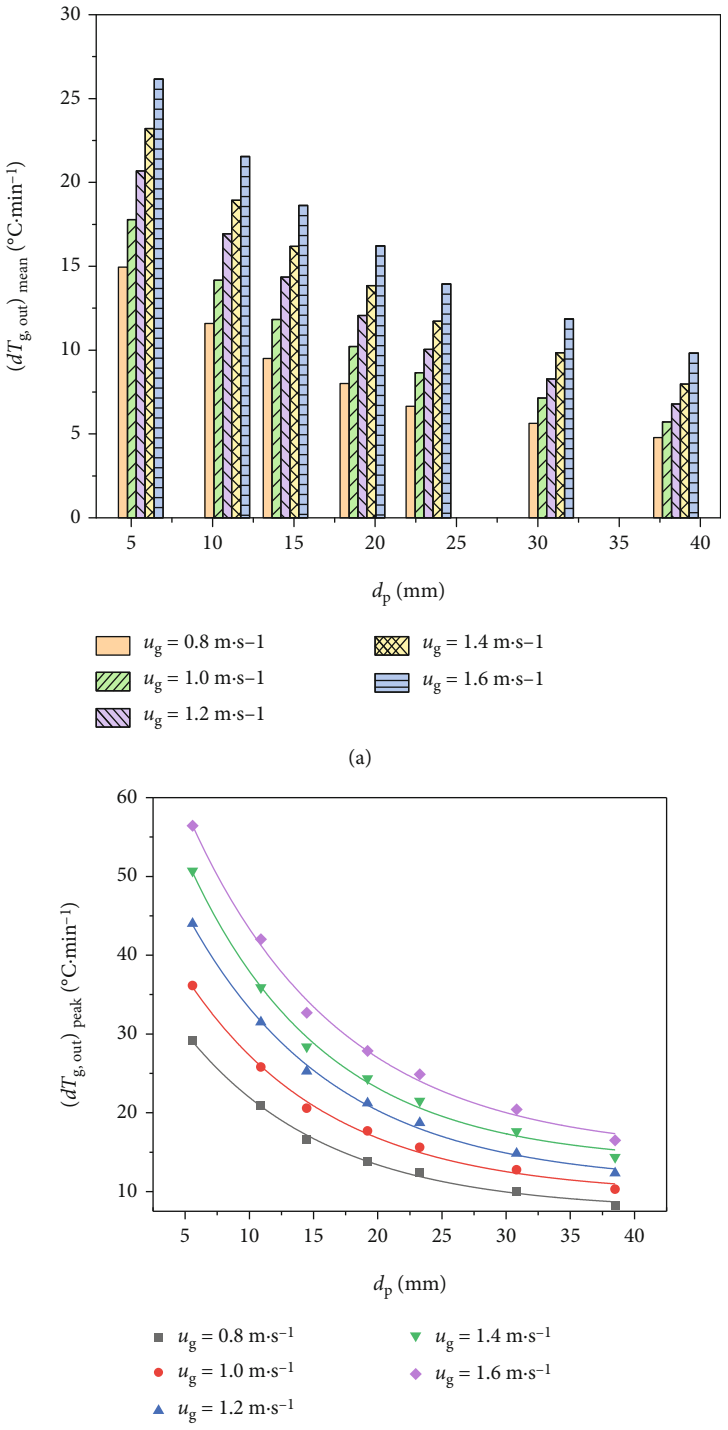

FIGURE 16: Change of the mean value $(dT_{g,out})_{mean}$ and peak value $((dT_{g,out})_{peak})$ of the change rate of the gas outlet temperature with the equivalent particle diameter d_p under different gas velocities u_g.

$$\mathrm{MRD}(\%) = \frac{1}{N}\sum_{i=1}^{N}\left|\frac{Nu_{cal,i} - Nu_{exp,i}}{Nu_{exp,i}}\right| \times 100, \qquad (13)$$

where Nu_{exp} and Nu_{cal} are the measured value and calculated value of the Nusselt number Nu, respectively.

First of all, the change trend of the measured value of the Nusselt number Nu is consistent with the predicted value obtained by this work, that is, it increases with the increase of the Reynolds number Re. Besides, the measured value is evenly distributed on both sides of the predicted curve with the mean relative deviation of only 7.61%. Therefore, the heat transfer correlation obtained by this paper can be used

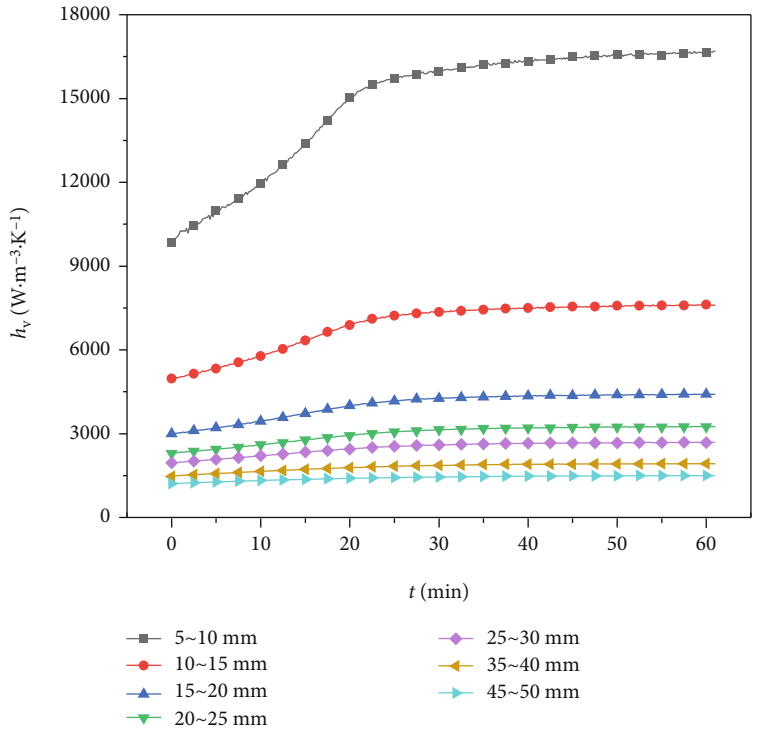

FIGURE 17: Variation of the volumetric heat transfer coefficient h_v with the cooling time t for the different kinds of sinters at the gas velocity of 0.8 m·s^{-1}.

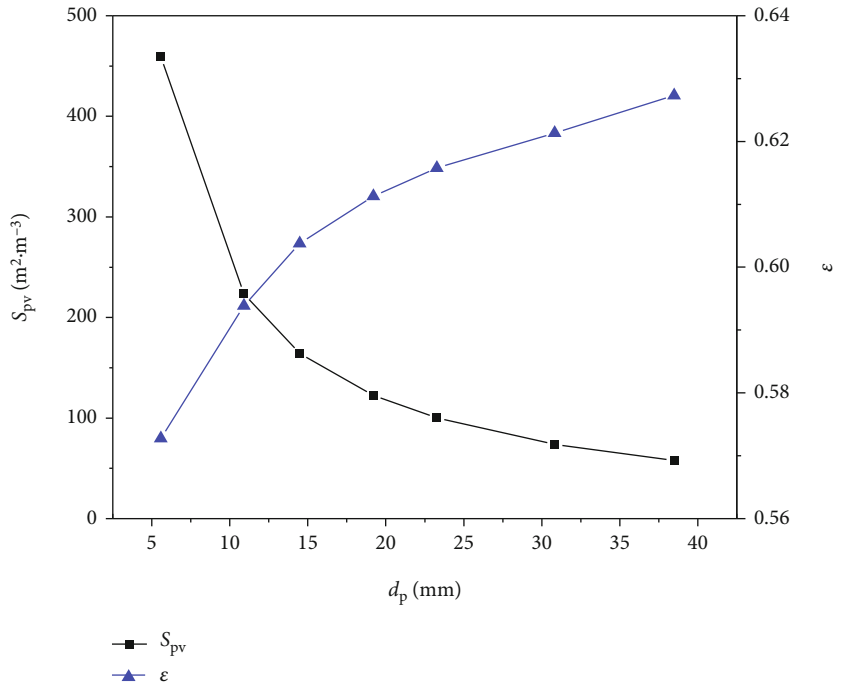

FIGURE 18: Variation of the specific surface area S_{pv} and bed voidage ε of sinter particles with the equivalent particle diameter d_p.

to accurately predict the gas-solid heat transfer characteristics in the sinter bed.

In addition, it is found that the variation of the measured value of the Nusselt number with the Reynolds number has the same trend as predicted values obtained by other works [9, 22–26, 40]. However, there is a considerable deviation in the value. Among them, the minimum value of MRD is 26.81%, and the maximum value of MRD is as high as 177.32%. This may be attributed to the different shape of packed particles in the bed. Compared with the previous

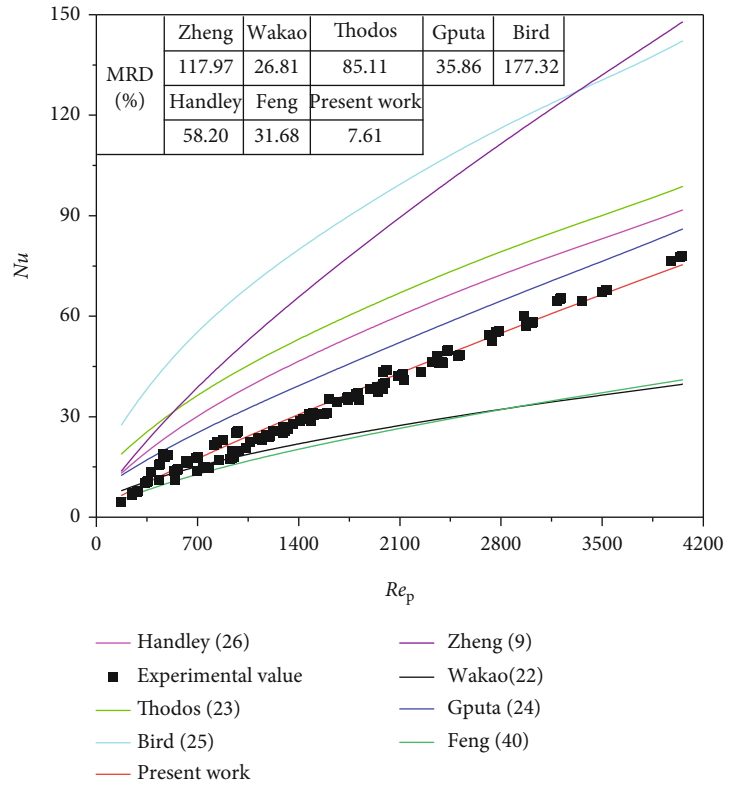

Figure 19: Comparison between the measured value of the Nusselt number Nu and predicted value of this work and other works.

particles, the shape of sinter particles is more irregular, resulting in different gas channels from regular particles [9]. Therefore, the heat transfer correlation of regular particles is no longer applicable to the sinter.

5. Conclusions

To establish an accurate model to optimize the vertical cooling process of the sinter, the key is to apply an accurate heat transfer correlation. Therefore, the heat transfer characteristics in the sinter bed with the typical particle size are experimentally studied. The inverse problem method is used to calculate the gas-solid heat transfer coefficient based on the gas outlet temperature, which is fitted into the correlation.

The results show that the heat transfer between the gas and sinter is significantly enhanced with the increase in the gas velocity. At the cooling time of 40 min, h_v increases from 16288 $W \cdot m^{-3} \cdot K^{-1}$ to 49599 $W \cdot m^{-3} \cdot K^{-1}$ with u_g increasing from 0.8 $m \cdot s^{-1}$ to 1.6 $m \cdot s^{-1}$, which increases by about twice. But this effect is gradually weakened with the increase in the particle size. With the particle size increasing from 5~10 mm to 45~50 mm, the slopes of the $(dT_{g,out})_{mean}$ curve and $(dT_{g,out})_{peak}$ curve decrease by 55.61% and 70.36%, respectively. In addition, the reduction of the particle size is also conducive to the enhancement of the heat transfer intensity. With the particle size decreasing, this effect is progressively evident. When the sinter is cooled to 40 min, the increasing extent of h_v is 1142.25 $W \cdot m^{-3} \cdot K^{-1}$ with the particle size decreasing from 20~25 mm to 15~20 mm, while that is 3152.65 $W \cdot m^{-3} \cdot K^{-1}$ with the particle size decreasing from 15~20 mm to 10~15 mm.

In addition, it is found that the variation of the measured value of the Nusselt number with the Reynolds number has the same trend as predicted values obtained by other works [9, 22–26, 40]. However, there is a considerable deviation in the value. Among them, the minimum value of MRD is 26.81%, and the maximum value of MRD is as high as 177.32%. It is proved that the previous empirical correlations are no longer applicable due to the difference of the shape. While the predicted value of this work is in good agreement with the measured value with the mean deviation of only 7.61%. Therefore, the modified correlation can accurately predict the gas-solid heat transfer characteristics in the sinter bed.

Nomenclature

c_p:	Specific heat capacity ($J \cdot kg^{-1} \cdot K^{-1}$)
d:	Particle size (m)
d_p:	Equivalent particle diameter (m)
h_v:	Volumetric heat transfer coefficient ($W \cdot m^{-3} \cdot K^{-1}$)
h_a:	Surface heat transfer coefficient ($W \cdot m^{-2} \cdot K^{-1}$)
L:	Bed height (m)
Nu:	Nusselt number (–)
Pr:	Prandtl number (–)
Re_p:	Particle Reynold number (–)
S_{pv}:	Specific surface area ($m^2 \cdot m^{-3}$)

T: Temperature (°C)
T_g, $T_{g,in}$, $T_{g,out}$: Gas temperature, inlet gas temperature, outlet gas temperature, respectively (°C)
$dT_{g,out}$: Change rate of the gas outlet temperature (°C·min^{-1})
T_s: Sinter temperature (°C)
t: Time (s)
u_g: Gas velocity (m·s^{-1})
z: Ordinate (m).

Greeks

ε: Bed voidage (–)
λ: Thermal conductivity (W·m^{-1}·K^{-1})
δ: Absolute error (–)
σ: Standard error (–)
ξ: Random number of the normal distribution (–)
ρ: Density (kg·m^{-3})
μ: Dynamic viscosity of the gas (Pa·s).

Subscripts

p: Particle
s: Sinter
g: Gas
err: Error
cal: Calculation
exp: Experiment.

Data Availability

The data used to support the findings of this study are included within the article.

Conflicts of Interest

The authors declare that they have no known competing financial interests or personal relationships that could have appeared to influence the work reported in this paper.

Acknowledgments

This work is supported by Fundamental Research Funds for the National Natural Science Foundation of China (Nos. 52006008 and 62033014).

References

[1] Q. Xu, K. Wang, Z. W. Zou et al., "A new type of two-supply, one-return, triple pipe-structured heat loss model based on a low temperature district heating system," *Energy*, vol. 218, article 119569, 2021.

[2] K. He and L. Wang, "A review of energy use and energy-efficient technologies for the iron and steel industry," *Renewable and Sustainable Energy Reviews*, vol. 70, pp. 1022–1039, 2017.

[3] Q. Xu, L. Liu, J. X. Feng et al., "A comparative investigation on the effect of different nanofluids on the thermal performance of two-phase closed thermosyphon," *International Journal of Heat and Mass Transfer*, vol. 149, article 119189, 2020.

[4] R. Q. Wang, L. Jiang, Y. D. Wang, and A. P. Roskilly, "Energy saving technologies and mass-thermal network optimization for decarbonized iron and steel industry: a review," *Journal of Cleaner Production*, vol. 274, article 122997, 2020.

[5] W. Chen, X. Yin, and D. Ma, "A bottom-up analysis of China's iron and steel industrial energy consumption and CO_2 emissions," *Applied Energy*, vol. 136, pp. 1174–1183, 2014.

[6] X. H. Zhang, Z. Chen, J. Y. Zhang, P. X. Ding, and J. M. Zhou, "Simulation and optimization of waste heat recovery in sinter cooling process," *Applied Thermal Engineering*, vol. 54, no. 1, pp. 7–15, 2013.

[7] H. Dong, L. Li, W. J. Liu, B. Wang, Y. S. Suo, and J. J. Cai, "Process of waste heat recovery and utilization for sinter in vertical tank," *China Metallurgy*, vol. 22, no. 1, pp. 6–11, 2012.

[8] K. Sun, C. Tseng, D. S. Wong et al., "Model predictive control for improving waste heat recovery in coke dry quenching processes," *Energy*, vol. 80, pp. 275–283, 2015.

[9] Y. Zheng, H. Dong, J. J. Cai et al., "Experimental investigation of volumetric heat transfer coefficient in vertical moving-bed for sinter waste heat recovery," *Applied Thermal Engineering*, vol. 151, pp. 335–343, 2019.

[10] C. G. Bi and J. J. Sun, "Application of process to recycle sensible heat of sinter using vertical cooling furnace in Meisteel," *Sintering and Pelletizing*, vol. 43, no. 4, pp. 69–72, 2018.

[11] J. S. Feng, H. Dong, J. Y. Liu, and K. Liang, "Gas-solid heat transfer characteristics in vertical tank for sinter," *CIESC Journal*, vol. 66, no. 11, pp. 4418–4423, 2015.

[12] Y. Liu, J. Y. Wang, Z. L. Cheng, J. Yang, and Q. W. Wang, "Experimental investigation of fluid flow and heat transfer in a randomly packed bed of sinter particles," *International Journal of Heat and Mass Transfer*, vol. 99, pp. 589–598, 2016.

[13] J. S. Feng, H. Dong, J. Y. Liu, K. Liang, and J. Y. Gao, "Experimental study of gas flow characteristics in vertical tank for sinter waste heat recovery," *Applied Thermal Engineering*, vol. 91, pp. 73–79, 2015.

[14] J. S. Feng, H. Dong, and H. D. Dong, "Modification of Ergun's correlation in vertical tank for sinter waste heat recovery," *Powder Technology*, vol. 280, pp. 89–93, 2015.

[15] J. S. Feng, S. Zhang, H. Dong, and G. Pei, "Frictional pressure drop characteristics of air flow through sinter bed layer in vertical tank," *Powder Technology*, vol. 344, pp. 177–182, 2019.

[16] F. Y. Tian, L. F. Huang, L. W. Fan et al., "Pressure drop in a packed bed with sintered ore particles as applied to sinter coolers with a novel vertically arranged design for waste heat recovery," *Journal of Zhejiang University-SCIENCE A*, vol. 17, no. 2, pp. 89–100, 2016.

[17] F. Y. Tian, L. F. Huang, L. W. Fan, H. L. Qian, and Z. T. Yu, "Wall effects on the pressure drop in packed beds of irregularly shaped sintered ore particles," *Powder Technology*, vol. 301, pp. 1284–1293, 2016.

[18] L. S. Pan, X. L. Wei, Y. Peng, X. B. Shi, and H. L. Liu, "Experimental study on convection heat transfer and air drag in sinter layer," *Journal of Central South University*, vol. 22, no. 7, pp. 2841–2848, 2015.

[19] S. Z. Zhang, Z. Wen, X. L. Liu, Y. Xing, and H. Zhang, "Gas flow characteristics through irregular particle bed with the vertical confined wall for waste heat recovery," *International Journal of Photoenergy*, vol. 2022, Article ID 1890541, 16 pages, 2022.

[20] S. Z. Zhang, "Effects of the layered distribution pattern on the gas flow resistance through the bed with the multisize irregular

particle for the waste heat recovery," *International Journal of Photoenergy*, vol. 2022, Article ID 3727937, 15 pages, 2022.

[21] S. Z. Zhang, Z. Wen, X. L. Liu, X. Liu, S. Wang, and H. Zhang, "Experimental study on the permeability and resistance characteristics in the packed bed with the multi-size irregular particle applied in the sinter vertical waste heat recovery technology," *Powder Technology*, vol. 384, pp. 304–312, 2021.

[22] N. Wakao, S. Kaguei, and T. Funazkri, "Effect of fluid dispersion coefficients on particle-to-fluid heat transfer coefficients in packed beds: correlation of nusselt numbers," *Chemical Engineering Science*, vol. 34, no. 3, pp. 325–336, 1979.

[23] A. S. Gupta and G. Thodos, "Mass and heat transfer in the flow of fluids through fixed and fluidized beds of spherical particles," *AICHE Journal*, vol. 8, no. 5, pp. 608–610, 1962.

[24] S. N. Gputa, R. B. Chaube, and S. N. Upadhyay, "Fluid–particle heat transfer in fixed and fluidized beds," *Chemical Engineering Science*, vol. 29, no. 3, pp. 839–843, 1974.

[25] M. V. Ramos, E. Kasai, J. Kano, and T. Nakamura, "Numerical simulation model of the iron ore sintering process directly describing the agglomeration phenomenon of granules in the packed bed," *ISIJ International*, vol. 40, no. 5, pp. 448–454, 2000.

[26] D. Handley and P. J. Heggs, "Momentum and heat transfer mechanisms in regular shaped packings," *Transactions of the Institution of Chemical Engineers*, vol. 46, pp. 251–264, 1968.

[27] W. E. Ranz, "Friction and transfer coefficients for single particles and packed beds," *Chemical Engineering Progress*, vol. 48, pp. 247–253, 1952.

[28] A. Singhal, S. Cloete, S. Radl, Q. F. Rosa, and S. Amini, "Heat transfer to a gas from densely packed beds of monodisperse spherical particles," *Chemical Engineering Journal*, vol. 314, pp. 27–37, 2017.

[29] J. B. Will, N. P. Kruyt, and C. H. Venner, "An experimental study of forced convective heat transfer from smooth, solid spheres," *International Journal of Heat and Mass Transfer*, vol. 109, pp. 1059–1067, 2017.

[30] J. Yang, J. Q. Wu, L. Zhou, and Q. W. Wang, "Computational study of fluid flow and heat transfer in composite packed beds of spheres with low tube to particle diameter ratio," *Nuclear Engineering & Design*, vol. 300, pp. 85–96, 2016.

[31] J. Q. Wu, J. Yang, L. Zhou, and Q. W. Wang, "Numerical analysis of fluid flow and heat transfer in various composite packed beds," *CIESC Journal*, vol. 66, pp. 111–116, 2015.

[32] J. Y. Wang, Q. Guo, J. Yang, Y. Liu, and Q. Wang, "Experimental study of convective heat transfer in grille-sphere composite structured packed bed," *Energy Procedia*, vol. 105, pp. 4782–4787, 2017.

[33] J. Y. Wang, J. Yang, Z. L. Cheng, Y. Liu, Y. Chen, and Q. Wang, "Experimental and numerical study on pressure drop and heat transfer performance of grille-sphere composite structured packed bed," *Applied Energy*, vol. 227, pp. 719–730, 2018.

[34] J. Yang, J. Wang, S. S. Bu, M. Zeng, and Q. W. Wang, "Experimental study of forced convective heat transfer in structured packed porous media of particles," *Journal of Engineering Thermophysics*, vol. 33, no. 5, pp. 851–855, 2012.

[35] J. Yang, Q. Wang, M. Zeng, and A. Nakayama, "Computational study of forced convective heat transfer in structured packed beds with spherical or ellipsoidal particles," *Chemical Engineering Science*, vol. 65, no. 2, pp. 726–738, 2010.

[36] J. Yang, J. Wang, S. S. Bu, M. Zeng, Q. Wang, and A. Nakayama, "Experimental analysis of forced convective heat transfer in novel structured packed beds of particles," *Chemical Engineering Science*, vol. 71, pp. 126–137, 2012.

[37] H. Tavassoli, E. A. J. F. Peters, and J. A. M. Kuipers, "Direct numerical simulation of fluid-particle heat transfer in fixed random arrays of non-spherical particles," *Chemical Engineering Science*, vol. 129, pp. 42–48, 2015.

[38] J. Jang and Y. Chiu, "3-D transient conjugated heat transfer and fluid flow analysis for the cooling process of sintered bed," *Applied Thermal Engineering*, vol. 29, no. 14-15, pp. 2895–2903, 2009.

[39] Z. C. Huang, Y. Yang, R. H. Zhong, Z. K. Liang, and B. Hu, "Heat transfer characteristics in process of hot sinter vertical cooling," *Iron and Steel*, vol. 54, no. 11, pp. 9–15, 2019.

[40] J. S. Feng, H. Dong, J. Y. Gao, J. Y. Liu, and K. Liang, "Experimental study of gas-solid overall heat transfer coefficient in vertical tank for sinter waste heat recovery," *Applied Thermal Engineering*, vol. 95, pp. 136–142, 2016.

[41] L. B. Younis and R. Viskanta, "Experimental determination of the volumetric heat transfer coefficient between stream of air and ceramic foam," *International Journal of Heat and Mass Transfer*, vol. 36, no. 6, pp. 1425–1434, 1993.

[42] J. J. Hwang, G. J. Hwang, R. H. Yeh, and C. H. Chao, "Measurement of interstitial convective heat transfer and frictional drag for flow across metal foams," *Journal of Heat Transfer*, vol. 124, no. 1, pp. 120–129, 2002.

[43] P. X. Jiang, R. N. Xu, and W. Gong, "Particle-to-fluid heat transfer coefficients in miniporous media," *Chemical Engineering Science*, vol. 61, no. 22, pp. 7213–7222, 2006.

[44] Q. Guo, Z. Wen, and R. Dou, "Experimental and numerical study on the transient heat-transfer characteristics of circular air-jet impingement on a flat plate," *International Journal of Heat and Mass Transfer*, vol. 104, pp. 1177–1188, 2017.

[45] J. S. Feng, H. Dong, S. Zhang, and L. Zhao, "Experimental study on gas-solid exergy transfer process in sinter vertical tank," *Journal of Iron and Steel Research*, vol. 32, no. 7, pp. 556–562, 2020.